Research on strip hysteretic behavior and mill vertical vibration system nonlinear dynamics

Xiaobin Fan[1] · Yong Zang[2] · Ke Jin[1]

Abstract Rolling mill vibration is a technical problem in the iron and steel industry for many years and has serious impact and harm on production. There were serious vibrations in the middle mills when rolling thin container strip for the compact strip production (CSP) strip hot rolling process. This paper studied the hysteretic characteristic of rolled strip and established the vertical vibration system single-degree-of-freedom dynamics model of the F3 mill rollers. The influence of parameters on the system characteristics was studied, such as the linear damping coefficient, linear stiffness coefficient, nonlinear displacement coefficient, nonlinear velocity coefficient and exciting force, and then, the vibration source and vibration-restraining measure were studied from the roll gap. The results show that with increasing linear stiffness, damping and hysteresis coefficient, it can reduce the possibility of chaotic system; the linear stiffness coefficient had the greatest influence, and hysteresis damping coefficient had minimal influence on chaotic threshold. In order to reduce rolling mill vibration amplitude, we should reduce the external excitation force firstly, and in order to improve the dynamic performance of the system, we should control the speed of nonlinear coefficient values. The contrast experiments were carried out at the production scene finally.

✉ Xiaobin Fan
fanxiaobin@hpu.edu.cn

[1] School of Mechanical and Power Engineering, Henan Polytechnic University, Jiaozuo 454003, China

[2] Mechanical Engineering Institute, University of Science and Technology Beijing, Beijing 100083, China

1 Introduction

Rolling mill vibration is a technical problem in iron and steel industry for many years and has serious impact and harm on production. Furumoto [1] designed a chamber in mill stabilizing device and optimized its size. Kim [2] modeled a rolling mill that includes the driving system by multibody dynamics to investigate the cause and characteristics of the chatter vibration. The chatter frequency was 1190 Hz and was caused by the rolling force. The amplitude of chatter vibration could be reduced by controlling the speed of the roll, and the static and dynamic components of the rolling force [2]. Swiatoniowski [3] presented a probabilistic model of the friction phenomena on the work/backup rolls contact surface and found that such character of the disturbance in distribution of zones with static and kinetic friction can be regarded as one of the sources of self-excited vibrations appearing in the system consisting of a rolling mill and a strip. Amer [4] studied the torsional vibration reduction for rolling mill's main drive system via negative velocity feedback under parametric excitation and found the resonance condition is the first natural frequency vibration, which is one of the worst resonance cases. Fujita proposed a new actuator for controlling the friction coefficient balance between the final stand and preceding stand as an intelligent hybrid lubrication control system for preventing chatter. The results show that the hybrid lubrication system can prevent chatter efficiently in high-speed cold-rolling region [5]. Kijima investigated the influence of lubrication on elongation and roughness transfer in skin-pass rolling by experimental rolling tests in which the relationship between lubrication behavior and the roll radius is clarified. It was found that operational size rolls can be explained convincingly by height characterization parameters and are considered to be reasonable, and some

characteristics of skin-pass rolling related to lubrication are not properly simulated using small radius, laboratory size rolls due to the insufficient contact length between the rolls and the workpiece [6]. Yildiz [7] developed a one-dimensional model and validated it against real plant data.

The CSP middle mills had severe vibration during rolling the thin container strip. So this paper studied the hysteretic characteristic of rolled strip and established the vertical vibration system single-degree-of-freedom dynamics model of the F3 mill rollers. The influence of parameters on the system characteristics was studied, such as the linear damping coefficient, linear stiffness coefficient, nonlinear displacement coefficient, nonlinear velocity coefficient and exciting force, and then, the vibration source and vibration-restraining measure were studied from the roll gap.

2 Rolled strip hysteresis model

CSP hot rolling is a large elastic–plastic deformation process, and under the dynamic load action, the strip will produce obvious hysteresis phenomenon, for example, loading and unloading path is different to form a hysteresis loop, as shown in Fig. 1. Hysteresis effect of rolled piece has great influence on rolling mill vibration system dynamics, and the rolling process shows that the influence of rolled piece type on rolling mill vibration is very obvious. So, it is necessary to further study the hysteretic characteristics of rolled piece under dynamic load and its crucial impact on rolling mill system dynamics. In order to establish the mathematical model reflecting hysteretic characteristic, we often consider that hysteresis loop is made as "base lines" of the elastic force and "pure hysteresis loop" of damping force; the area of hysteresis loop is equal to the energy work of one cycle [8]. There are some commonly used hysteretic models such as bilinear model, polynomial model and the differential equation control model.
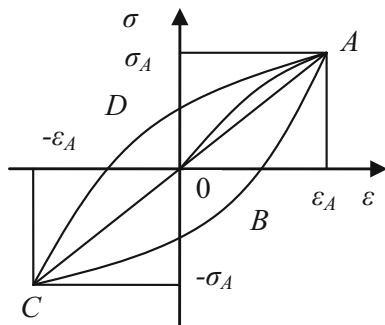

Fig. 1 Ideal hysteresis loop under dynamic load

2.1 Bilinear model

Bilinear model is presented based on the ideal dry friction model and is shown in Fig. 2; the relationship between restoring lag force $F(y)$ and displacement is indicated as double broken line, and its expression is as follows:

$$F(y) = \begin{cases} b_1 + k_1 y & y < 0 \quad \dot{y} > 0 \\ b_2 + k_2 y & y > 0 \quad \dot{y} > 0 \\ b_3 + k_3 y & y > 0 \quad \dot{y} < 0 \\ b_4 + k_4 y & y < 0 \quad \dot{y} < 0 \end{cases} \tag{1}$$

To simplify the calculation, the model can be approximately linearized and acquired equivalent stiffness k_e and equivalent damping c_e, namely

$$\begin{aligned} k_e = \frac{1}{\pi A} \Bigg[&\int_0^{\phi_D} (b_3 + k_1 A \cos \varphi) \cos \varphi \, \mathrm{d}\varphi \\ &+ \int_{\phi_D}^{\pi} (b_4 + k_2 A \cos \varphi) \cos \varphi \, \mathrm{d}\varphi \\ &+ \int_{\pi}^{\phi_B} (b_1 + k_1 A \cos \varphi) \cos \varphi \, \mathrm{d}\varphi \\ &+ \int_{\phi_B}^{2\pi} (b_2 + k_2 A \cos \varphi) \cos \varphi \, \mathrm{d}\varphi \Bigg] \end{aligned}$$

$$\begin{aligned} c_e = \frac{1}{\pi A} \Bigg[&\int_0^{\phi_D} (b_3 + k_1 A \cos \varphi) \sin \varphi \, \mathrm{d}\varphi \\ &+ \int_{\phi_D}^{\pi} (b_4 + k_2 A \cos \varphi) \sin \varphi \, \mathrm{d}\varphi \\ &+ \int_{\pi}^{\phi_B} (b_1 + k_1 A \cos \varphi) \sin \varphi \, \mathrm{d}\varphi \\ &+ \int_{\phi_B}^{2\pi} (b_2 + k_2 A \cos \varphi) \sin \varphi \, \mathrm{d}\varphi \Bigg] \end{aligned}$$
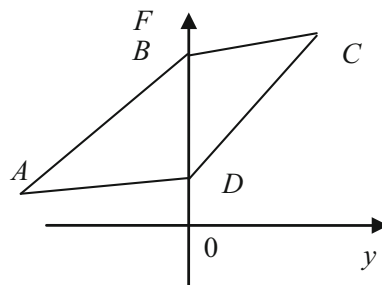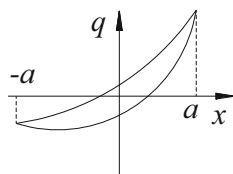

Fig. 2 Bilinear model

Fig. 3 Hyperbolic function model

where A is the amplitude, x_B and x_D are vibration displacement corresponding to point B and point B, respectively. There are $\varphi_B = \arccos \frac{x_B}{A}$ and $\varphi_D = \arccos \frac{x_D}{A}$. The hysteresis model is substituted into the vibration differential equation, and the approximate solution of system can be obtained by incremental method as follows:

$$x = a\cos\phi + \frac{b}{6\pi}\sin 3\phi + \cdots + 4\frac{b}{n(n^2-1)\pi}\sin n\phi, \quad (2)$$
$$n = 3, 5, 7 \ldots$$

where b is the constant. From the equation, we found there are not even-order harmonics in the higher harmonic in its solution, which is not consistent with the rolling mill vibration field test results [9]. So, it is not suitable for double linear model to describe the hysteretic characteristic of rolled piece.

2.2 Polynomial model

Due to point mutations in bilinear model and making the hysteresis loop more smoother, we can adopt hyperbolic functions and exponential functions such as polynomial hysteresis model. Among them, the load curve q_1 and discharge curve q_2 of hyperbolic function are shown in Fig. 3.

$$q_1 = \rho_1 + \frac{x}{\beta_1 + \beta_2 x}, \quad \dot{x} > 0 \quad \text{and}$$
$$q_2 = -\rho_2 + \frac{x}{\beta_1 - \beta_3 x}, \quad \dot{x} \le 0 \quad (3)$$

In order to solve differential equation expediently, the load curve q_1 and discharge curve q_2 are expressed as nth derivative, namely

$$q_1^{(n)} = \frac{(-1)^{n-1} n! \beta_1 \beta_2^{n-1}}{(\beta_1 - \beta_2 x)^{n+1}}, \quad \dot{x} > 0 \quad \text{and}$$
$$q_2^{(n)} = \frac{n! \beta_1 \beta_3^{n-1}}{(\beta_1 - \beta_3 x)^{n+1}}, \quad \dot{x} \le 0 \quad (4)$$

Taking 2th power series, there are $q_1 = \rho_1 + \frac{x}{\beta_1} - \frac{2\beta_2}{\beta_1^2}x^2$, $\dot{x} > 0$ and $q_2 = -\rho_2 + \frac{x}{\beta_1} + \frac{2\beta_3}{\beta_1^2}x^2$, $\dot{x} \le 0$. According to Fig. 3, loading and unloading curves are equivalent at a location, that is $q_1(a) = q_2(a)$. And there was the following equation:

$$\rho_1 + \frac{a}{\beta_1} - \frac{2\beta_2}{\beta_1^2}a^2 = -\rho_2 + \frac{a}{\beta_1} + \frac{2\beta_3}{\beta_1^2}a^2 \quad (5)$$

Setting $k = \frac{1}{\beta_1}$, $d = \frac{2\beta_2}{\beta_1^2}$, $\lambda d = \frac{2\beta_3}{\beta_1^2}$, $\rho_1 = -\frac{2\beta_2}{\beta_1^2}a^2$, $-\rho_2 = -\frac{2\beta_3}{\beta_1^2}a^2$ and substituting it into Eq. (5), we get the loading and unloading curves of hyperbolic function as follows:

$$q_1(x) = kx + d(a^2 - x^2), \quad \dot{x} > 0 \quad \text{and}$$
$$q_2(x) = kx - \lambda d(a^2 - x^2), \quad \dot{x} \le 0 \quad (6)$$

where d is the nonlinear coefficient, λ is the asymmetric coefficient (when $\lambda = 1$, loading and unloading curves are symmetrical about the origin). If the hysteresis curve is expressed as a exponential equation and obtained the various derivatives, there are following equations:

$$q_1 = be^{rx} + \rho_1, \quad \dot{x} > 0, \quad q_1^{(n)} = br^n e^{rx}, \quad \dot{x} > 0$$
$$q_2 = ce^{sx} - \rho_2, \quad \dot{x} \le 0, \quad q_2^{(n)} = cs^n e^{sx}, \quad \dot{x} \le 0 \quad (7)$$

where ρ_1, ρ_2, b, c, r and s are test constants. The above equations are expressed as power series form and take $n = 2$; there are following equations:

$$q_1 = b + \rho_1 + brx + \frac{1}{2}br^2 x^2, \quad \dot{x} > 0 \quad \text{and}$$
$$q_2 = c - \rho_2 + csx + \frac{1}{2}cs^2 x^2, \quad \dot{x} \le 0 \quad (8)$$

Setting $k = br$, $k_2 = \frac{1}{2}br^2$, $c_1 = b + \rho_1$, $\lambda = \frac{cs^2}{br^2}$, $c_2 = -c + \rho_2$ and substituting it into above equations, there are following equations:

$$q_1 = c_1 + kx + k_2 x^2 \quad \text{and} \quad q_2 = -c_2 + kx + \lambda k_2 x^2 \quad (9)$$

By $q_1(a) = q_2(a)$ and setting $c_1 = c_2$, then Eq. (9) can be expressed as follows:

$$q_1 = \frac{1}{2}(\lambda - 1)k_2 a^2 + kx + k_2 x^2 \quad \text{and}$$
$$q_2 = -\frac{1}{2}(\lambda - 1)k_2 a^2 + kx + \lambda k_2 x^2 \quad (10)$$

In engineering calculation, we can use Davidenkov model to describe the sluggish by the constitutive equation, which is shown in Fig. 4, and the equation is expressed as follows:

$$\sigma^{\mp} = E\left\{ u \mp \frac{\eta}{n}\left[(u_0 \mp u)^n - 2^{n-1}u_0^n \right] \right\} \quad (11)$$

where σ is the normal stress, u is the strain, η is the hysteresis loop coefficient, n is the hysteresis loop index, "$\mp$" signifies the first half and second half curve, respectively. The greater η, the distance between the loading and unloading curve is greater, and the greater n, the hysteresis loop curve is closer to the elastic–plastic hysteresis loop.

In order to solve the equation easily, the lag nonlinear force is also expressed as cubic function of displacement
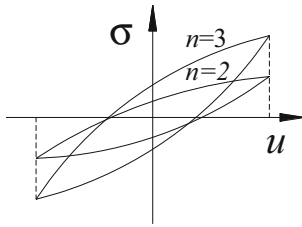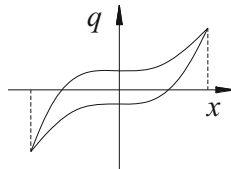
Fig. 4 Davidenkov model

Fig. 5 Cubic function model

and velocity, namely $F(x, \dot{x}) = ax^3 + bx^3$, which is shown in Fig. 5. And by adjusting the values of a and b, we can obtain good fitting effect.

2.3 Differential equation control model

Bouc and Wen put forward the Bouc–Wen model controlled by differential equation [10], and the model has good versatility and parameter identification performance relative to bilinear model and curve model, in which the nonlinear restoring force $G(x, \dot{x})$ is consisted of two parts, namely $G(x, \dot{x}) = h(x, \dot{x}) + \chi z(x, \dot{x})$, where $h(x, \dot{x})$ is the non-hysteretic constraining force; it is a function of the transient displacement and velocity, its expression is $c_0 \dot{x} + k_0 x$; $z(x, \dot{x})$ is hysteretic constraining force and was determined by the following equation:

$$\dot{z} = Ax - \alpha|\dot{x}||z|^{n-1}z - \beta\dot{x}|z|^n \tag{12}$$

where A, n, α and β are the parameters determining the shape and smooth degree of hysteresis loop. If the lag force F_p is determined by Bouc–Wen the model, there are only odd times frequency such as three times and five times, which do not agree with the test results, so it is not suitable for the control differential equation model. In addition, the commonly used hysteresis models are Ramberg–Osgood and Menegotto–Pinto model suitable for different situations [11].

3 Hysteresis nonlinear vertical vibration dynamics

3.1 Single-degree-of-freedom vertical vibration model and the parameters influence

According to the rolling mill structure feature and the measured results, the single-degree-of-freedom delayed parametrically excited vibration model was set up as shown

Fig. 6 Single-DOF nonlinear model
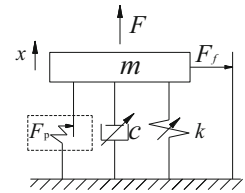
in Fig. 6 (ignoring friction F_f between the bearing seat and the mill house), and the motion differential equation is expressed as follows:

$$m\ddot{x} + c\dot{y} + k(1 + \gamma\cos 2\Omega\tau)y + Ay^3 + B\dot{y}^3 = F\cos\Omega\tau \tag{13}$$

where m is the roll system weight, c is the linear damping, k is the linear stiffness, A is the displacement nonlinear constant, B is the speed nonlinear constant, $\Omega/51$ is the roll rotation frequency, and F is the excitation force.

The system can be considered as a weak nonlinear system with small damping, and we introduce small parameter ε and tuning parameter σ. For the main resonance, setting $\Omega = \sqrt{k/m}$, $\delta = 1 + 2\varepsilon\sigma$, $t = \tau \cdot \sqrt{k/m}$, $x = y \cdot \sqrt{A/k}$, the dimensionless equation is as follows:

$$\ddot{x} + x = \varepsilon\left(-\frac{8}{3}\alpha x^3 - \frac{8}{3}\beta\dot{x}^3 - \mu\dot{x} - 2\sigma x - 4x\cos 2t\right) + \varepsilon^2 f\cos t \tag{14}$$

If the first-order approximation solving the equation is $x = a\cos\varphi$, where $\varphi = pt + \theta$, after the equation K-B transformation, there is

$$\begin{cases} \dfrac{\mathrm{d}a}{\mathrm{d}t} = -\beta a^3 - \mu a + a\sin 2\theta \\ \dfrac{\mathrm{d}\theta}{\mathrm{d}t} = -\alpha a^2 + \sigma + \cos 2\theta \end{cases} \tag{15}$$

For the steady motion, there are $\frac{\mathrm{d}a}{\mathrm{d}t} = 0$ and $\frac{\mathrm{d}\theta}{\mathrm{d}t} = 0$, and according to the Eq. (15), after θ elimination, there are

$$\begin{cases} a = 0 \\ c_4 a^4 + c_2 a^2 + c_0 = 0 \end{cases} \tag{16}$$

where $c_4 = \alpha^2 + \beta^2$, $c_2 = 2(\sigma\alpha + \mu\beta)$, $c_0 = \sigma^2 + \mu^2 - 1$. The influence of linear damping coefficient μ, the displacement nonlinear coefficient α and velocity nonlinear coefficient β on the amplitude frequency characteristics curve of main resonance are shown in Fig. 7. And we can see the linear damping coefficient μ not only affects the main resonance curve shape, but also the size, and the smaller damping coefficient the worse system stability. The displacement nonlinear coefficient α only affects primary resonance curve shape. The smaller the velocity nonlinear coefficient β, the greater the main resonance amplitude, and the influence relation is clear.

The parameters influence on the system dynamic time domain response was also studied. The system response
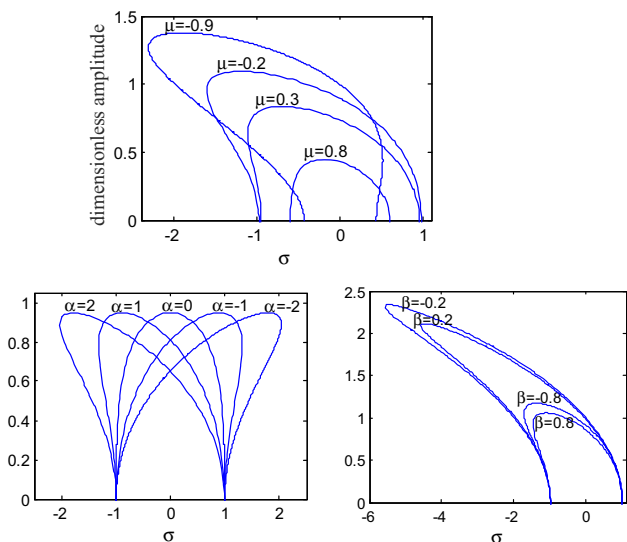
Fig. 7 System parameters influence on the amplitude frequency characteristic

curves are shown in Fig. 8 with linear stiffness coefficient 4×10^9 N m^{-1} (Fig. 8a) and 4×10^{11} N m^{-1} (Fig. 8b). There are displacement response graph, phase diagram, power spectra, Poincaré section and hysteresis force diagram in Fig. 8. And we can see the system vibration amplitude decreases obviously after linear stiffness coefficient increase, but energy is more concentrated. From the phase diagram, power spectra and Poincaré section, the system has quasi-periodic motion.

The system Lyapunov exponent curve corresponding to Fig. 8a is shown in Fig. 9, and we can see the index is negative, namely the system is in non-chaotic state. The system amplitude bifurcation curves based on linear stiffness coefficient are shown in Fig. 10, and we can see with the increase in linear stiffness coefficient, the vibration amplitude has volatility, but did not produce bifurcation.

The system response curves with linear damping coefficient 3×10^6 N s m^{-1} (Fig. 11a) and 3×10^7 N s m^{-1} (Fig. 11b) are shown in Fig. 11, and the subgraphs are displacement response, phase diagram, power spectra, Poincare section and hysteresis force diagram, respectively. And we can see with the increase in linear damping coefficient, system lag force is increased and the hysteresis loop shape was almost unchanged; the vibration amplitude significantly declined, but oscillation state unchanged, for example, the linear damping coefficient can help to reduce the vibration intensity increase. The Lyapunov exponent curve is shown in Fig. 12 with the linear damping coefficient c taking 8.8×10^6 N s m^{-1}; we can see Lyapunov exponent is negative, for example, the system is not in chaotic state. The system amplitude bifurcation curve by linear damping coefficient is shown in Fig. 13; we can see with the rise of the linear damping coefficient, the vibration
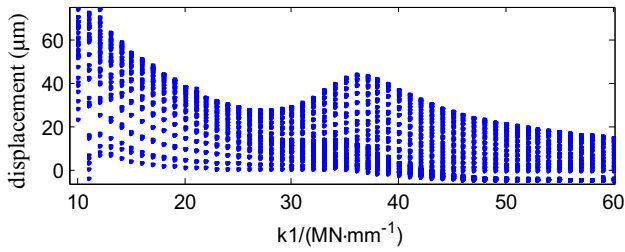

(a)

(b)
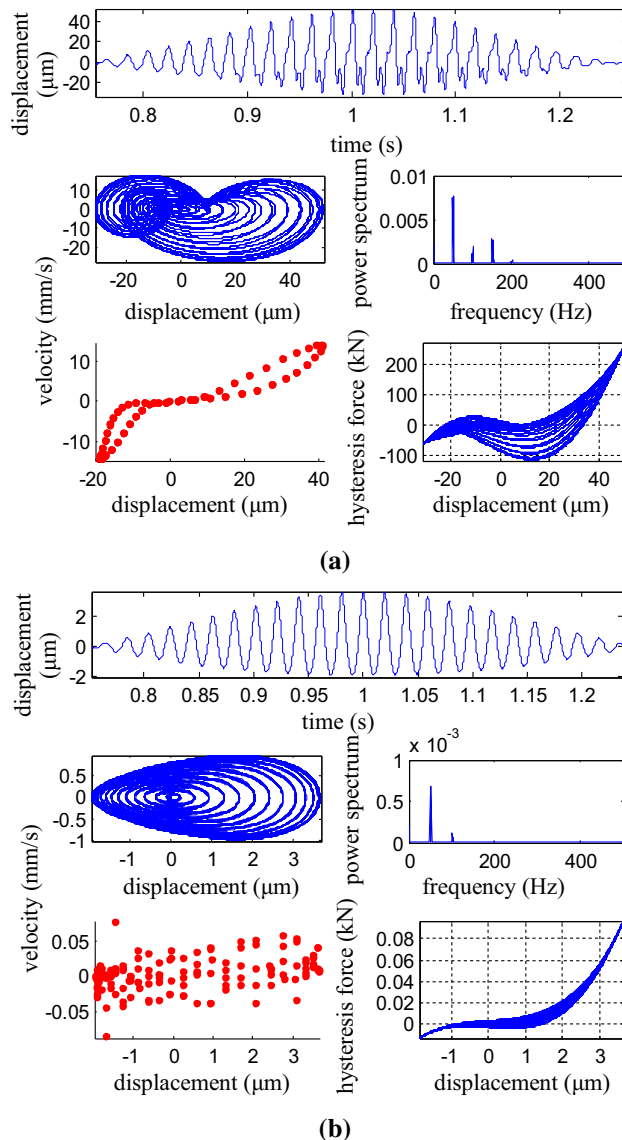
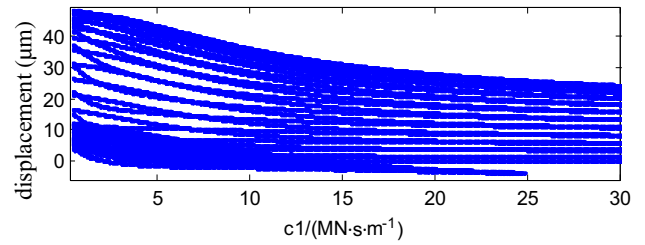Fig. 8 The influence of linear stiffness coefficient on the system response
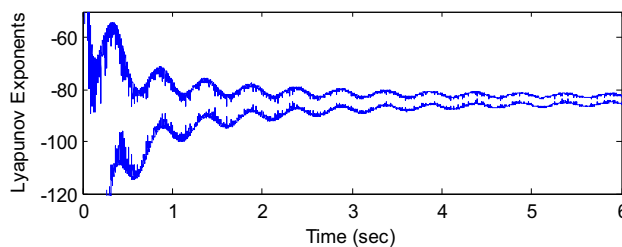
Fig. 9 Lyapunov exponents

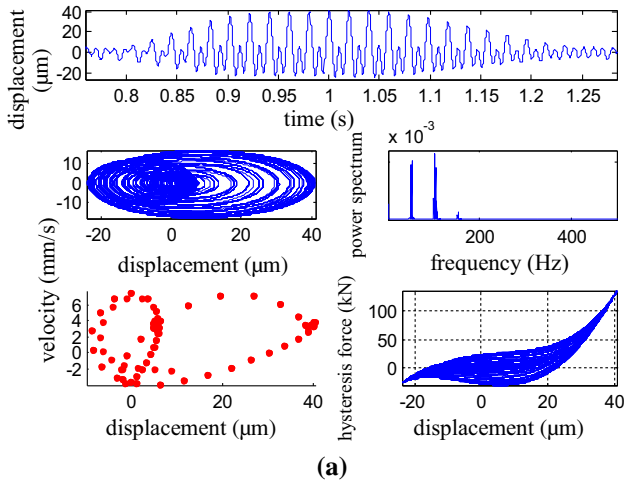amplitude has declined, but did not produce bifurcation phenomenon.

The system response curve is shown in Fig. 14 with the displacement nonlinear coefficient A 2×10^{17} N m^{-3} (Fig. 14a) and 2×10^{19} N m^{-3} (Fig. 14b), and the
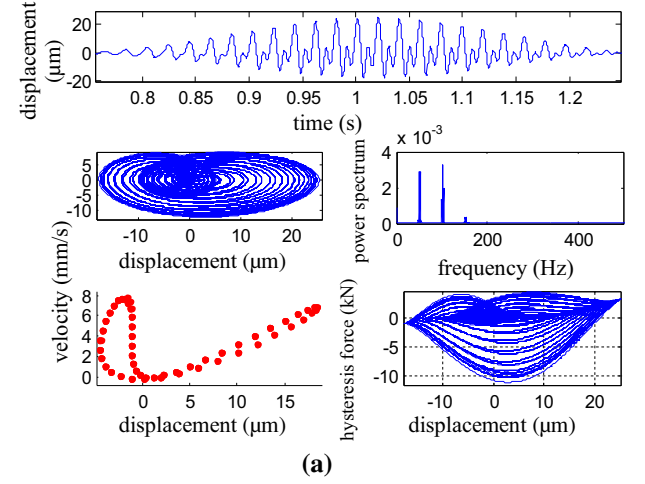
Fig. 10 Displacement linear coefficient bifurcation
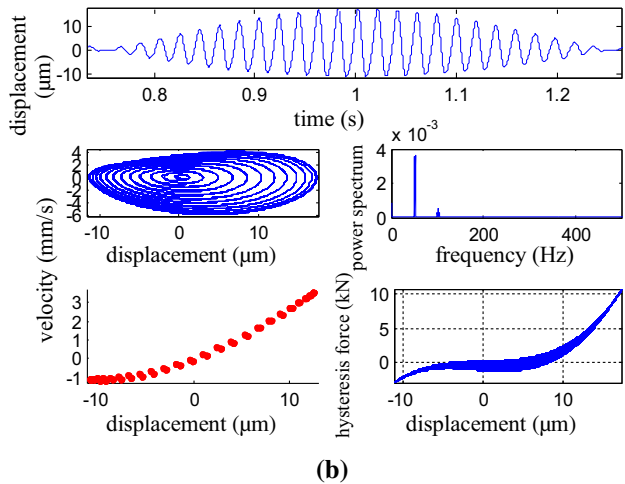

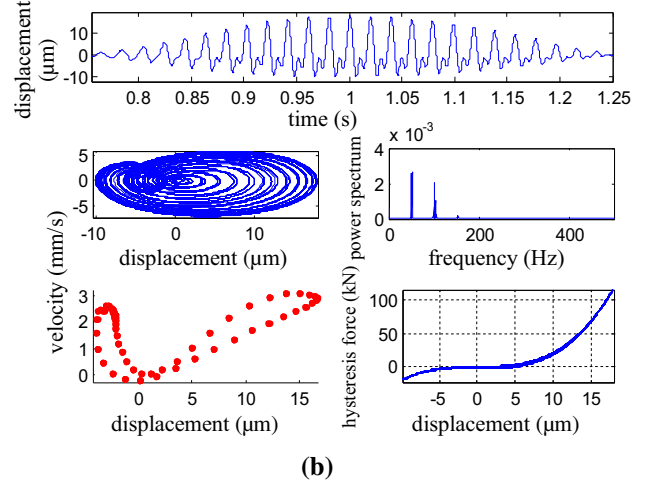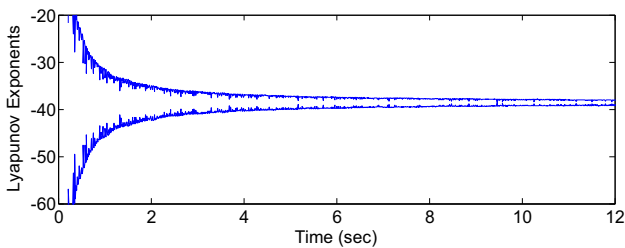**Fig. 13** Linear damping coefficient bifurcation

(a)

(a)

(b)

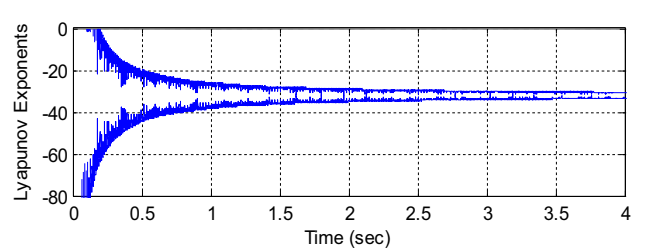**(b)**

Fig. 11 Linear damping coefficient influence

Fig. 14 Displacement nonlinear coefficient effect

Fig. 12 SYSTEM LYAPUNOV EXPOnents
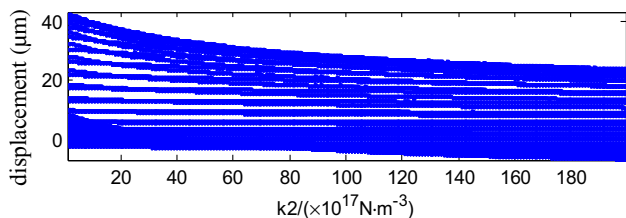

Fig. 15 System Lyapunov exponents

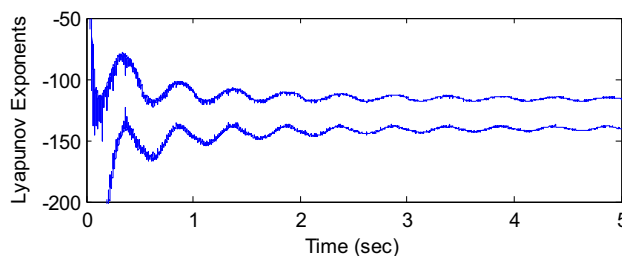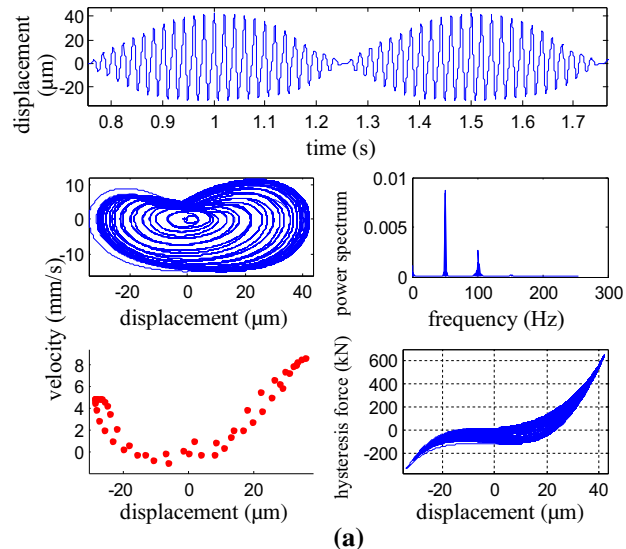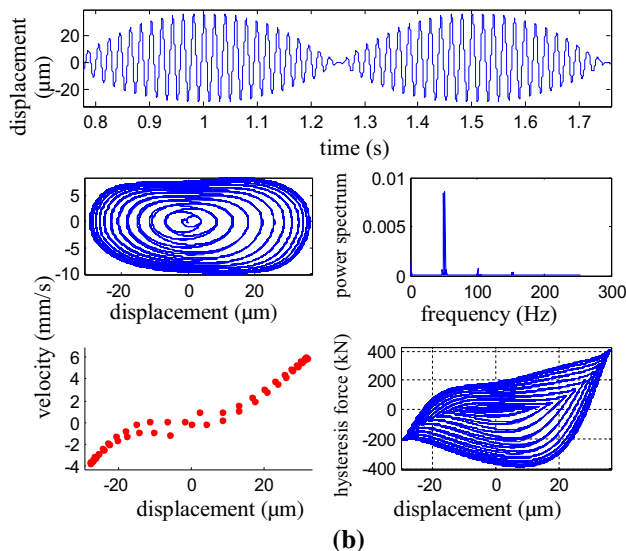**Fig. 16** Displacement nonlinear coefficient bifurcation

Fig. 17 Velocity nonlinear coefficient influence

Fig. 18 Lyapunov exponents curve

Fig. 19 Velocity coefficient nonlinear bifurcation

subgraphs are displacement response, phase diagram, power spectra, Poincare section and hysteresis force diagram, respectively. We can see that after the displacement nonlinear coefficient increases, vibration amplitude decreases, hysteresis loop becomes narrow, and the hysteresis effect decreases; Lyapunov exponent is shown in Fig. 15, and we can see Lyapunov exponent is negative, so
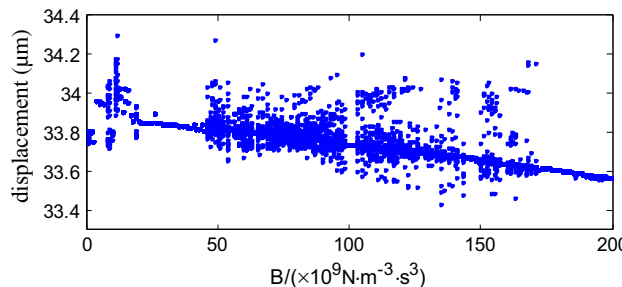
the system is not chaotic. The amplitude bifurcation curve based on the displacement nonlinear coefficient is shown in Fig. 16; we can see the amplitude does not produce bifurcation phenomenon and amplitude increases as the displacement nonlinear coefficient decreases.

The system response curve is shown in Fig. 17 with velocity nonlinear coefficient B 6×10^9 N s^{-3} m^{-1} (Fig. 17a) and 6×10^{11} N s^{-3} m^{-1} (Fig. 17b), and we can see with the velocity nonlinear coefficient increase, the vibration amplitude decreases obviously, the hysteresis loop becomes fat, and the hysteresis effect enhances; Lyapunov exponents curve is shown in Fig. 18, and Lyapunov exponent is negative and is not chaotic. The amplitude bifurcation curve by nonlinear coefficient is shown in Fig. 19; as the velocity nonlinear coefficient increases, the amplitude produces bifurcation phenomenon, for example, velocity nonlinear coefficient has a great influence on the system dynamics.

The system response curve with the roller rotation frequency ($\Omega/51$) 0.5 Hz (Fig. 20a) and 1.5 Hz (Fig. 20b) is shown in Fig. 20. We can see with the excitation frequency increase, vibration amplitude has significant increase and hysteresis loop becomes fat. The system Lyapunov exponents curve is shown in Fig. 21, Lyapunov exponents value is negative, and the system is not chaotic. The vibration amplitude bifurcation curve by excitation frequency is shown in Fig. 22, and it can be seen there are some bifurcation phenomena.

The system response curve is shown in Fig. 23 with excitation force F 5×10^5 N (Fig. 23a) and 5×10^6 N

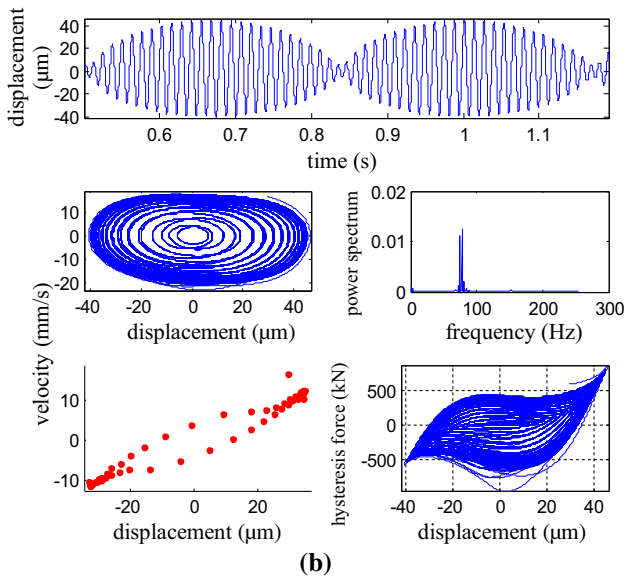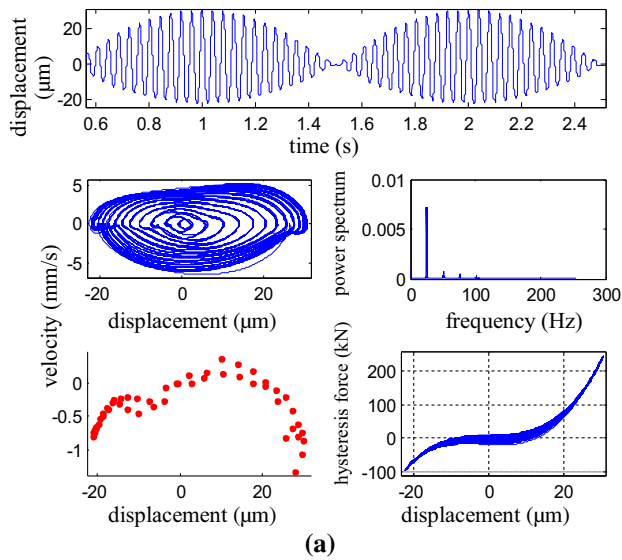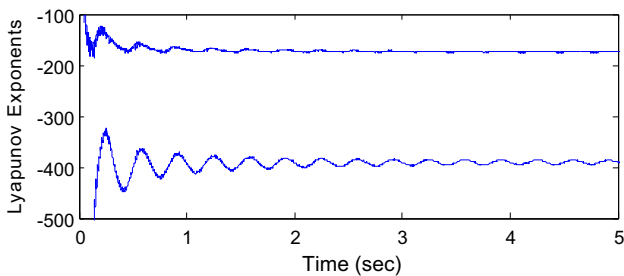**Fig. 20** The excitation frequency influence

Fig. 21 System Lyapunov exponents

Fig. 22 Excitation frequency bifurcation

Fig. 23 Excitation force influence

(Fig. 23b); we can see with the excitation force increase, vibration amplitude increases obviously and hysteresis loop becomes narrow. Lyapunov exponents curve is shown in Fig. 24, the Lyapunov exponents is negative, and the
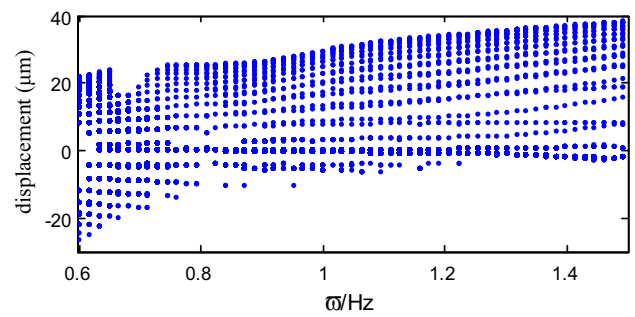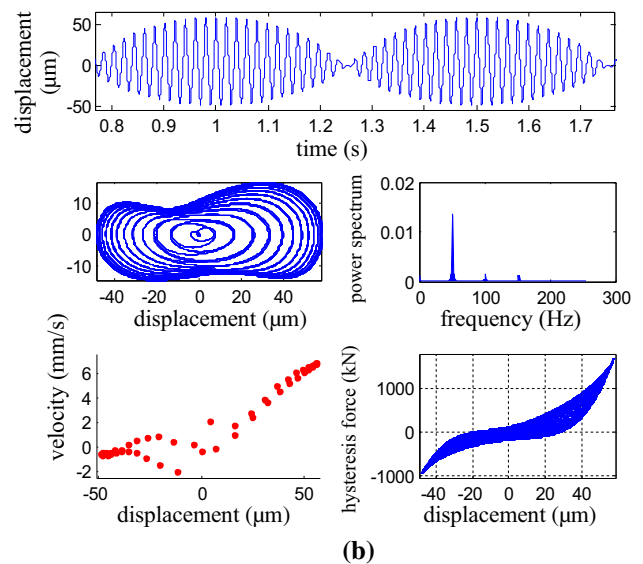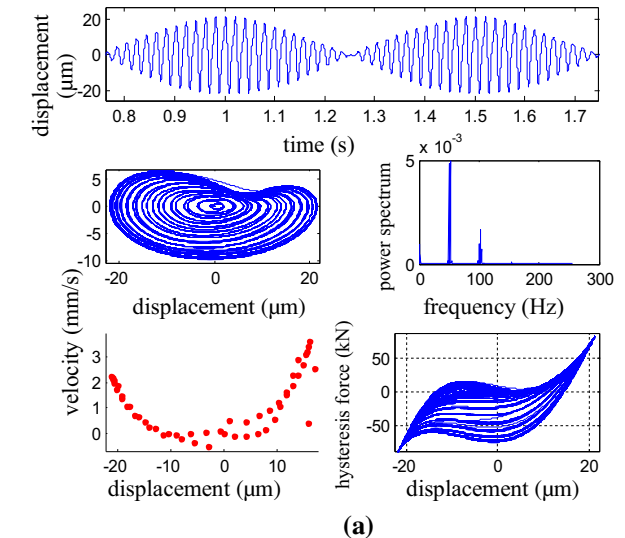
system is not chaotic; vibration amplitude bifurcation curve by excitation force is shown in Fig. 25, and we can see vibration amplitude produces some bifurcation phenomenon with the excitation amplitude increase.
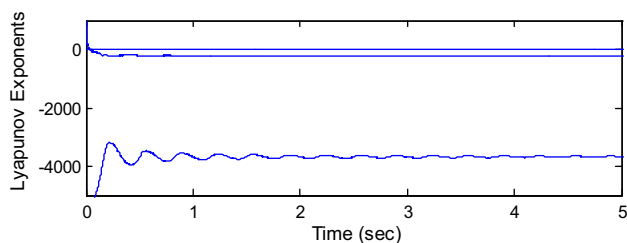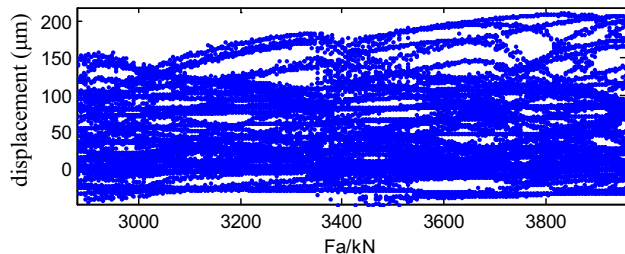
Fig. 24 System Lyapunov exponents

Fig. 25 Excitation force bifurcation

3.2 The vertical vibration system stability analysis and chaos threshold calculation

Stability research methods on the linear time-invariant control systems are Routh–Hurwitz criterion, Nyquist criterion and Evans root locus method, etc. And the research on the stability of the nonlinear system is more complicated; the commonly used methods are graphical method, algebraic criterion method and Lyapunov direct method, etc.

When there is slight perturbation of the initial state on the power system, the disturbance with time will be increased or reduced at a rate index, the index rate is known as the characteristic index or Lyapunov exponents, and it is the best way to describe the high sensitivity to initial value. Lyapunov stability theory is determined based on energy concept, and it needs to find or construct a Lyapunov function $V(x,t)$ and study the time differential along the state trajectory. For n-dimensional discrete dynamical system, $X_{k+1} = F(X_k)$, set $\{X_k\}$ is a track of the system, and ΔX_k is a small amount deviate from the track. If the evolution of ΔX_k satisfies $\Delta X_{k+1} = \left(\frac{\partial F}{\partial X}\big|_{X=X_k}\right)\Delta X_k = J_k \Delta X_k$, where J_k is the *Jacobian* matrix of F at X_k, and there are $\Delta X_{k+1} = J_k \Delta X_k = J_k J_{k-1\cdots} J_1 \Delta X_1$. Set $J^{(k)} = J_k J_{k-1} \cdots J_1$, then $\Delta X_{k+1} = J^{(k)} \Delta X_1$, positive definite matrix $T(X) = \lim_{k\to\infty}\left(\left(J^{(k)}\right)^T J^{(k)}\right)^{\frac{1}{2k}}$,, where $\lambda_1 \geq \lambda_2 \geq \cdots \geq \lambda_n > 0$ is n eigenvalue of $T(x)$, and Lyapunov exponents λ of the system is as follows:

$$\lambda = \lim_{n\to\infty}\frac{1}{n}\sum_{i=1}^{n}\ln\lambda_i \quad (i = 1, 2, \ldots, n) \tag{17}$$

When $\lambda < 0$, adjacent points become close and merge into one point, which is corresponding to the stable fixed point and periodic motion. When $\lambda > 0$, adjacent points will separate, which is corresponding to the local instability of orbit and can be used as the chaos criterion.

For n-dimensional continuous dynamic system, the system forms a track $x(t, x_0)$ at the initial conditions x_0. If the initial conditions have small changes $\delta x(x_0, 0)$, the track deviation is $\delta x(x_0, t) = x(t, x_0 + \delta x(x_0, 0)) - x(t, x_0)$ at t moment. At $t = 0$, setting x_0 as the center, make n-dimensional spherical surface by radius $\|\delta x(x_0, 0)\|$. Because the shrinkage or expansion degree of each direction is different, with the time evolution, the sphere will evolve into n-dimensional ellipsoid at t moment. Setting the half-axis length of the ellipsoid along the ith coordinate axis direction as $\|\delta x_i(x_0, t)\|$, the ith Lyapunov exponents σ_i of the system is as follows:

$$\sigma_i = \lim_{t\to\infty}\frac{1}{t}\ln\frac{\|\delta x_i(x_0,t)\|}{\|\delta x_i(x_0,0)\|} \quad (i = 1, 2, \ldots, n) \tag{18}$$

If the system Lyapunov Exponents Li < 0, the system has constant movement; if L1 = 0 and Li < 0, the system has periodic motion; if L1 = L2 = 0 and Li < 0, the system has prevail periodic motion; if Li > 0, the system has chaotic motion; if Li is endless, the system has random movement. The system of maximum Lyapunov exponents greater than zero usually is a chaotic system, and these systems have high sensitive dependencies to initial conditions of tiny change, for example Lorenz equation, Logistic mapping and the Hénon mapping are chaotic systems. These chaotic systems have the following characteristics, the chaotic attractor in phase space has boundary on the whole, the phase trajectory has high instability in the attractor, and the dimensions of the strange attractor are fractional. The chaos research methods have phase track diagram direct observation, Poincare section, Lyapunov exponents analysis and fractal dimension analysis method, etc.

According to the analysis of Sect. 3.1, we study the mill vertical vibration system chaos movement with exciting force as bifurcation parameter. Considering the friction between the bearing seat and the memorial arch, rolling mill vibration system dynamic equation can be expressed as follows:

$$m\ddot{x} + kx + c\dot{x} + Ax^3 + B\dot{x}^3 + \mu F_N \cdot \text{sign}(\dot{x}) = P_A \cos \Omega t \tag{19}$$

where A and B are the hysteresis loop coefficients, μ is the friction coefficient between the bearing and memorial arch, and F_N is the normal pressure. Introducing the variables: $\omega^2 = \frac{k}{m}$, $H_1 = \frac{A}{m}$, $H_2 = \frac{c}{m}$, $H_3 = \frac{B}{m}$, $H_4 = \frac{\mu F_N}{m}$, $F' = \frac{P_A}{m}$, and

substituting them into Eq. (19), there is the following equation:

$$\ddot{x} + \omega^2 x + H_1 x^3 + H_2 \dot{x} + H_3 \dot{x}^3 + H_4 \cdot \text{sign}(\dot{x}) = F' \cos \Omega t \tag{20}$$

Setting $a = \frac{F'}{\Omega^2}$, $y = \frac{x}{a}$, $T_1 = \frac{1}{\omega}$, $T_2 = \frac{1}{H_2}$, $\tau = \frac{t}{T_1}$, $\varepsilon = \frac{T_1}{T_2}$ and substituting them into Eq. (20), then after dimensionless processing, then there is the following equation:

$$\frac{d^2 y}{d\tau^2} + y + d_1 y^3$$
$$+ \varepsilon \left[\frac{dy}{d\tau} + d_2 \left(\frac{dy}{d\tau} \right)^3 + d_3 \text{sign}\left(\frac{dy}{d\tau} \right) - d_4 \cos\left(\frac{\Omega}{\omega} \tau \right) \right] = 0 \tag{21}$$

where $d_1 = \frac{H_1 a^2}{\omega^2}$, $d_2 = \frac{H_3 a^2 \omega^2}{H_2}$, $d_3 = \frac{H_4}{a \omega H_2}$, $d_4 = \frac{\Omega^2}{\omega H_2}$. Converting Eq. (21) to state equation and expressed into matrix form (τ is expressed as t): $\dot{Y} = f(Y) + \varepsilon g(Y, t)$, there are the following equation:

$$f(Y) = \begin{pmatrix} y_2 \\ -y_1 - d_1 y_1^3 \end{pmatrix},$$
$$g(Y, t) = \begin{pmatrix} 0 \\ -y_2 - d_2 y_2^3 - d_3 \text{sign}(y_2) + d_4 \cos\left(\frac{\Omega}{\omega} t \right) \end{pmatrix}$$

When $\varepsilon = 0$, it is a conservative system. For $d_1 > 0$, the undisturbed movement is a stable periodic motion, and there is no chaos under Smale meaning; For $d_1 < 0$, the system has three fixed points: $O_1(0, 0)$, $O_2\left(\sqrt{-\frac{1}{d_1}}, 0 \right)$, $O_3\left(-\sqrt{-\frac{1}{d_1}}, 0 \right)$, O_2 and O_3 are saddle point.

The Hamilton function is established as H: $H = \frac{y_2^2}{2} + \frac{y_1^2}{2} + \frac{d_1 y_1^2}{4}$. The lodge track meets $H = \frac{y_2^2}{2} + \frac{y_1^2}{2} + \frac{d_1 y_1^2}{4} = -\frac{1}{4d_1}$ through the saddle points O_2 and O_3, and we can get y_1 after substituting $y_2 = \frac{dy_1}{dt}$ into the formula and separating the variables and integration. Then substituting y_1 into $y_2 = \frac{dy_1}{dt}$, we can work out y_2, and the two final different lodge orbit expressions are as follows:

$$\begin{cases} y_1(t) = \pm \sqrt{-\frac{1}{d_1}} \tan h \left(\sqrt{\frac{1}{2}} t \right) \\ y_2(t) = \pm \sqrt{-\frac{1}{2d_1}} \sec h^2 \left(\sqrt{\frac{1}{2}} t \right) \end{cases} \tag{22}$$

Substituting Eq. (22) into the system Melnikov function and after integration, there is following equation:

$$M(t_0) = \int_{-\infty}^{\infty} f(q_0(t)) \wedge g(q_0(t), t + t_0) dt$$
$$= \int_{-\infty}^{\infty} y_2(t) \left[-y_2(t) - d_2 y_2^3(t) - d_3 \text{sign}(y_2(t)) \right.$$
$$\left. + d_4 \cos \frac{\Omega}{\omega}(t + t_0) \right] dt$$
$$= \frac{2\sqrt{2}}{3d_1} - \frac{8\sqrt{2}d_2}{35d_1^2} \mp 2d_3 \sqrt{\frac{1}{-d_1}} \text{sign}(\dot{y})$$
$$\pm \frac{d_4 \sqrt{\frac{1}{-d_1}} \pi \Omega \csc h \left(\frac{\pi \Omega}{2\sqrt{2}\omega} \right) \sec h \left(\frac{\pi \Omega}{2\sqrt{2}\omega} \right) \sin \left(\frac{\Omega t_0}{\omega} \right)}{\sqrt{2}\omega}$$

If making $M(t_0) = 0$ and considering $\left| \sin\left(\frac{\Omega t_0}{\omega} \right) \right| \leq 1$ and $\frac{dM(t_0)}{dt_0} \neq 0$, it will be expected to have the following equation.

$$2d_3 \sqrt{\frac{1}{-d_1}} - \frac{2\sqrt{2}}{3d_1}$$
$$+ \frac{8\sqrt{2}d_2}{35d_1^2} < \frac{d_4 \sqrt{\frac{1}{-d_1}} \pi \Omega \csc h \left(\frac{\pi \Omega}{2\sqrt{2}\omega} \right) \sec h \left(\frac{\pi \Omega}{2\sqrt{2}\omega} \right)}{\sqrt{2}\omega} \tag{23}$$

According to Melnikov function theorem, when Eq. (23) is satisfied, there has t_0 nothing to do with ε, which makes the system have cross-sectional homoclinic points, that is, there may be chaotic solution. So when the system produces chaos, we can get extraneous force amplitude (equivalent to eccentricity a) threshold as follows:

$$a > \frac{2\omega^3 \sqrt{-\frac{1225H_1^2 H_2^2 - 840H_1 H_2 H_3 \omega^4 + 144H_3^2 \omega^8}{H_1^2}} \sin h \left(\frac{\pi \Omega}{\sqrt{2}\omega} \right)}{105\sqrt{H_1} \pi \Omega^3} \overset{\text{def}}{\Rightarrow} F(\Omega) \tag{24}$$

Setting parameters: $m = 1.1 \times 10^5$ kg, $k = 2.5 \times 10^{10}$ N/m, $c = 4 \times 10^6$ N s/m, $A = -5 \times 10^{16}$ N/m^3, $B = -5 \times 10^5$ N s^3/m^3, $\Omega = 51 \times 2\pi$(rad/s), $a = P_A/(m\Omega^2)$, $\mu F_N = 0.1 \times 5 \times 10^5$ N, $P_A = 0.5 \times 10^6$ N.

Through changing the values of k, c, A and B, we can see the system chaos threshold change condition shown in Fig. 26. When a is under the curve, the system does not produce chaos. With the increase in k, c, A and B, it can reduce the possibility of chaos system. Among them, the parameter of the smallest influence on the chaos threshold is B and the largest is k.

4 Rolling mill vibration field test

From on-site inspection, we found the F3 mill reducer active gear produced crack; obviously, it has a certain relationship with rolling mill vibration, so the F3
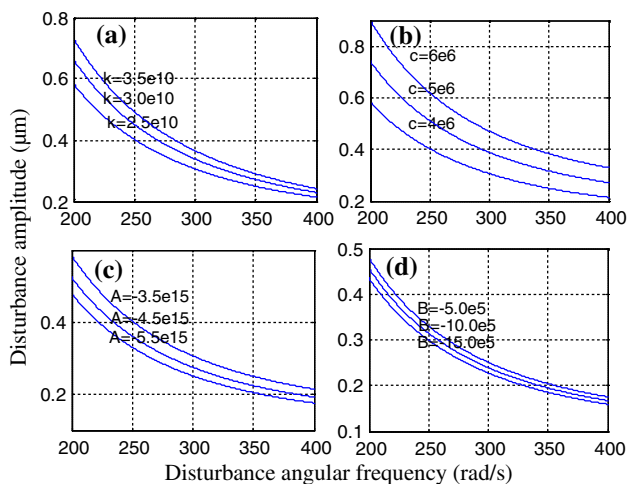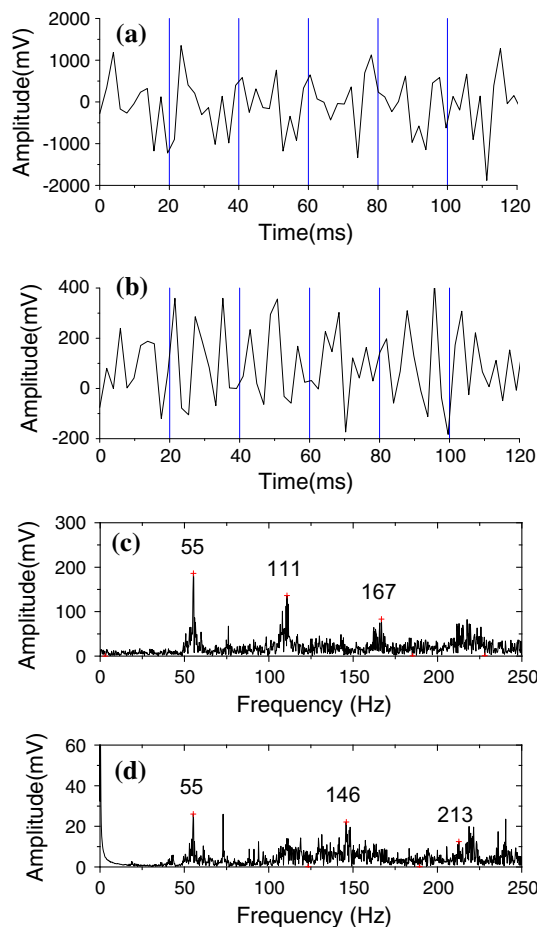
Fig. 26 The relationship between mill parameter and chaotic critical condition
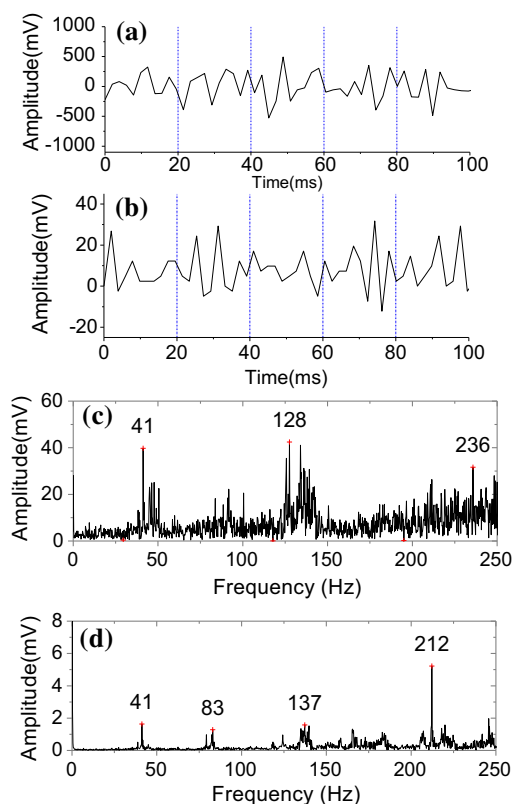
Fig. 27 Work roll (**a**, **c**) and reducer (**b**, **d**) vertical vibration time and frequency curve with thick strip

Fig. 28 Work roll (**a**, **c**) and reducer (**b**, **d**) vertical vibration time and frequency curve with thin strip

reducer and the work roller vertical vibration were tested synchronously. The vibration curves of time domain and frequency domain are shown in Fig. 27 for 4.5-mm-thick plate (no vibration sense of rolling work rolls) on the F3 (figure a) and reducer (figure b). The vibration curves of time domain and frequency domain are shown in Fig. 28 for 1.6-mm-thin plate (vibration sense strong of rolling work rolls) on the F3 (Fig. 28a) and reducer (Fig. 28b).

From Fig. 27, the vertical vibration energy of the work roll and speed reducer is relatively dispersive with no vibration sense, both have peak in 41 Hz and double frequency, the vibration forms are basically same, and only vibration amplitude is different (work roll vibration energy is much larger than reducer), for example, the vibration relationship between them is obvious. From Fig. 28, vibration energy is relatively concentrated with strong vibration sense and mainly distributed in 55 Hz and its double frequency, the roll vibration amplitude is more than twice than rolling thick plate, and vibration amplitude of reducer is more than 10 times than thick plate, that is, the vibration intensity increase of the reducer is more intense, the vibration damage to the gear reducer is more serious, so suppressing vibration is the important way to increase the service life of gear reducer. We can see with the finishing thickness thinning, the roll speed increases from 39 to 64 r/min, and the vibration frequency has increased from 41 to 55 Hz. Obviously, vibration main frequency and rolling speed have linear relationship approximately.

5 Conclusions

In order to study the effect of each parameter on the system dynamics and reduce calculation cost, the system is simplified into single-degree-of-freedom nonlinear model and was simulated. The results show that with increasing linear stiffness, damping and hysteresis coefficient, it can reduce the system chaotic possibility. The linear stiffness coefficient had the greatest influence, and hysteresis damping coefficient had minimal influence on chaotic threshold. In order to reduce rolling mill vibration amplitude, we should reduce the external excitation force firstly, and in order to improve the dynamic performance of the system, we should control the speed of nonlinear coefficient values. Field experiments show that the rolling mill vibration and the gear meshing impact excitation have a very significant influential relationship.

References

1. H. Furumoto, S. Kanemori, K. Hayashi, A. Sako, T. Hiura, H. Tonaka, Enhancing technologies of stabilization of mill vibration by mill stabilizing device in hot rolling. Proced. Eng. **81**, 102–107 (2014)
2. Y. Kim, K. Chang-Wan, L. Sung-Jin, H. Park, Experimental and numerical investigation of the vibration characteristics in a cold rolling mill using multibody dynamics. ISIJ Int. **52**(11), 2042–2047 (2012)
3. Andrzej Swiatoniowski, Ryszard Gregorczyk, Self-excited vibrations in four-high rolling mills caused by stochastic disturbance of friction conditions on the roll-roll contact surface. Mech. Control **29**(3), 158–162 (2010)
4. Y.A. Amer, A.T. El-Sayed, F.T. El-Bahrawy, Torsional vibration reduction for rolling mill's main drive system via negative velocity feedback under parametric excitation. J. Mech. Sci. Technol. **29**(4), 1581–1589 (2015)
5. N. Fujita, Y. Kimura, K. Kobayashi, K. Itoh, Y. Amanuma, Y. Sodani, Dynamic control of lubrication characteristics in high speed tandem cold rolling. J. Mater. Process. Technol. **229**, 407–416 (2015)
6. H. Kijima, An experimental investigation on the influence of lubrication on roughness transfer in skin-pass rolling of steel strip. J. Mater. Process. Technol. **225**(3), 1–8 (2015)
7. S.K. Yildiz, J.F. Forbes, B. Huang, Y. Zhang, F. Wang, V. Vaculik, Dynamic modelling and simulation of a hot strip finishing mill. Appl. Math. Model. **33**(7), 3208–3225 (2009)
8. B. Armstrong-Hélouvry, Stick slip and control in low-speed motion. IEEE Trans. Autom. Control **38**(10), 1483–1496 (1993)
9. Fan Xiaobin, *Vibration Problem Research for CSP Mill Stand [D]* (University of Science and Technology Beijing, Beijing, 2007)
10. Y.K. Wen, Method for random vibration of hysteretic system. J. Eng. Mech. Div. **102**(2), 249–263 (1976)
11. A. Niesłony, C.E. Dsoki, H. Kaufmann, P. Krug, New method for evaluation of the manson–coffin–basquin and ramberg–osgood equations with respect to compatibility. Int. J. Fatigue **30**, 1967–1977 (2008)